A Study of Particle Histories During Spray Drying Using Computational Fluid Dynamic Simulations

C. Anandharamakrishnan[+], J. Gimbun, A.G.F. Stapley* and C.D. Rielly

Department of Chemical Engineering, Loughborough University

Loughborough, Leicestershire, LE11 3TU, UK

---

*Correspondence: A.G.F. Stapley, Department of Chemical Engineering, Loughborough University, Loughborough, Leicestershire, LE11 3TU, UK

*Tel:+44-1509-222525, E. Mail: A.G.F.Stapley@lboro.ac.uk

[+] Present address: Central Food Technological Research Institute, Mysore-570020, India

Abstract

Computational fluid dynamics (CFD) models for short-form and tall-form spray dryers have been developed, assuming constant rate drying and including particle tracking using the source-in-cell method. The predictions from these models have been validated against published experimental data and other simulations. This study differs from previous work in that particle time-histories for velocity, temperature and residence time and their impact positions on walls during spray drying have been extracted from the simulations. Due to wet-bulb protection effects, particle temperatures are often substantially different from gas temperatures, which is important, since the particle temperature-time history has the most direct impact on product quality. The CFD simulation of an existing tall-form spray dryer indicated that more than 60% of the particles impacted on the cylindrical wall and this may adversely affect product quality, as solids may adhere to the wall for appreciable times, dry out and lose their wet-bulb protection. The model also predicts differences between the particle primary residence time distributions (RTD) and the gas phase RTD. This study indicates that a short form dryer with a bottom outlet is more suitable for drying of heat sensitive products, such as proteins, due to the low amounts of recirculated gas and hence shorter residence time of the particles.

Keywords: Spray-drying, particle velocity and temperature, residence time, impact positions.

INTRODUCTION

Spray drying is a well established method for converting liquid feed materials into a dry powder form[1, 2]. Spray drying is widely used to produce powdered food products such as whey, instant coffee, milk, tea and soups, as well as healthcare and pharmaceutical products, such as vitamins, enzymes and bacteria[1]. In recent years, computational fluid dynamics (CFD) has been increasingly applied to food processing operations[3, 4]. For spray-drying, CFD simulation tools are now often used because measurements of air flow, temperature, particle size and humidity within the drying chamber are very difficult and expensive to obtain in large-scale dryers.

A number of articles have been published on CFD simulations of spray drying [5-8] (see also the review by Langrish and Fletcher[9]). Both the Eulerian-Eulerian and Eulerian-Lagrangian two-phase models have been used in published simulations of spray drying. Here, the Eulerian-Lagrangian framework was selected because it allows tracking of individual particles and hence provides residence times for a wide range of particle sizes; generally such a simulation method is suitable for relatively low volume fractions of the dispersed phase, *e.g.* for spray-drying applications. Lagrangian tracking with a reasonable number of particles may be performed using the "particle source in cell" (PSI-Cell) model, which includes two-way coupling between the drying gas and the spray particles[10]. The PSI-Cell model was used by Papadakis and King[11], who found good agreement between model and experimental results in a co-current spray dryer. Huang *et al.*[8] also used this method in their comparison of spray

drying using rotary and pressure nozzles. However, although existing studies have used particle tracking methods in performing simulations, no studies have presented data relating to the particle histories themselves. An exception was Kieviet[12], who studied the airflow pattern, temperature, humidity, particle trajectories and residence times in a co-current spray dryer fitted with a pressure nozzle. It should be noted, however, that Kieviet's[12] 2-D axi-symmetric model did not consider swirl and recirculation and was not able to represent accurately the real chamber geometry, which was asymmetric due to the outlet pipe exiting from the side of the chamber cone[8].

Relatively, few articles have been published on particle histories during spray drying. Woo *et al*. [13] simulated particle surface moisture contents using Reaction Engineering Approach (REA) and characteristic drying curve (CDC) methods and they found that both the models predicts almost similar particle moisture and trajectories. Recently, Jin and Chen[14] studied the effects of particle size on particle residence time using REA. However, particle temperature data along with residence time and impact positions are the most important results that can be derived from a spray drying simulation, especially if the product is heat sensitive (*e.g.* proteins, enzymes and cells). In Eulerian-Lagrangian simulations these data are accessible and can be extracted from the CFD software using post-processing software to investigate particle time-histories, trajectories and impact positions. Such data will now be reported here for two systems:

Case A: Short-form spray dryer simulation is conducted using the same geometry and boundary conditions as Kieviet's[12] experimental study. This same system was also simulated by Huang *et al.*[8] using particle tracking via the source-in-cell method. Case A thus serves as a useful validation of the model set-up.

Case B: After validating the model in Case A, attention is focused on modelling a tall-form spray dryer used in a previous study of protein denaturation[15] to gain further insight into how and where denaturation might occur in this system.

The main weakness of the model is that due to processing constraints only a simple constant rate-drying model was used in these simulations. Accordingly, the results should be interpreted by acknowledging that in practice drying rates will be lower and temperatures correspondingly higher for particles in the latter stages of drying.

SPRAY DRYING CFD SIMULATION METHODOLOGY

The CFD code Fluent 6.3 was used to simulate two co-current flow spray-dryers, one fitted with a hydraulic pressure nozzle (*Case A)* and one using an air blast (pneumatic) atomiser (*Case B).* The simulations were performed in a three dimensional geometry assuming steady state conditions for air flow and particle injection. In Case A, a three-dimensional (3D) model was created in GAMBIT; a hexahedral mesh (typical mesh size 0.001 m) was used for the cylindrical part of the drying chamber, whereas at the bottom of the cone chamber a tetrahybrid

mesh was used (mesh size also 0.001 m) due to meshing problems in the outlet pipe. The number of grid cells used was 295,090. In Case B, a 3D-model was created in GAMBIT; a hexahedral grid (typical mesh size 0.001 m) was used throughout, with 294,237 grid cells. Preliminary tests showed that this number of cells was sufficient to ensure a grid independent prediction of the mean velocity field.

Fluent employs the finite volume method to solve the partial differential forms of the continuity and the Reynolds-Averaged Navier-Stokes equations using the SIMPLE (Semi-Implicit Pressure-Linked Equations) method for pressure-velocity coupling and a second-order upwind scheme to interpolate the variables on the surface of the control volume. Particle Lagrangian tracking was realized via a discrete phase model (DPM) model with two-way coupling between the continuous flow and particle;[16] *i.e.,* there is a feedback mechanism in which the continuous and dispersed phase flows interact. The standard k-ε model was employed as a turbulence closure method. The k and ε inlet values were calculated using the equations given by Langrish and Zbicinski[17].

The combined Eulerian-Lagrangian model was used to obtain particle trajectories by solving the force balance equation between particle momentum, drag and buoyancy:

$$\frac{d\underline{u}_p}{dt} = \left(\frac{18\mu}{\rho_p d_p^2}\right)\frac{C_D\, Re}{24}\left(\underline{v} - \underline{u}_p\right) + \underline{g}\left[\frac{\rho_p - \rho_g}{\rho_p}\right] \qquad (1)$$

where, $\underline{v}$ is the fluid phase velocity vector, $\underline{u_p}$ is the particle velocity vector, ρ_g is the density of the fluid and ρ_p is the density of the particle.

The slip Reynolds number (*Re*) and drag coefficient (C_D) are given by the following equations

$$Re = \frac{\rho_g d_p \left| \underline{v} - \underline{u}_p \right|}{\mu} \tag{2}$$

$$C_D = a_1 + \frac{a_2}{Re} + \frac{a_3}{Re^2} \tag{3}$$

where, d_p is the particle diameter and a_1, a_2 and a_3 are constants that apply to smooth spherical particles over several ranges of *Re* given by Morsi and Alexander[18].

Turbulent particle dispersion was included in this model using the discrete eddy concept (details are provided in the Fluent manual[16]). In this approach, the turbulent air flow pattern is assumed to be made up of a collection of randomly directed eddies, each with its own lifetime and size. Particles are injected into the flow domain at the nozzle point and envisaged to interact with the mean flow and with these random eddies until they impact the wall or leave the flow domain through the product outlet; thus each particle experiences a stochastic effect on its trajectory. In this study, particle stickiness and particle-particle collisions (agglomeration) were not considered.

The species transport model was selected within the DPM to enable the prediction of simultaneous heat and mass transfer to and from the particle during the drying process. Thus heat and mass transfer effects between the particles and the hot gas allowed particle temperature and moisture content time-histories to be calculated. The heat transfer equation is:

$$\frac{d}{dt}\left(m_p c_p T_p\right) = hA_p\left(T_g - T_p\right) + \frac{dm_p}{dt} h_{fg} \tag{4}$$

where, m_p is the mass of the particle, c_p is the particle specific heat capacity, T_p is the particle temperature, h_{fg} is the latent heat of vaporisation, A_p is the surface area of the particle and h is the heat transfer coefficient.

The mass transfer rate (for evaporation) between the gas and the particles was calculated from the following equation.

$$\frac{dm_p}{dt} = -k_c A_p\left(Y_s^* - Y_g\right) \tag{5}$$

where, Y_s^* is the saturation humidity, Y_g is the gas humidity and k_c is the mass transfer coefficient.

The values of vapour pressure, density, specific heat and diffusion coefficients were obtained from various sources[19,20] and used as piece-wise linear functions of temperature in this model. In the event that the temperature of the particle reaches the boiling point and whilst the mass of the particle exceeds the non-volatile fraction, the boiling rate model was applied [16].

$$\frac{\mathrm{d}d_p}{\mathrm{d}t} = \frac{4k_{ta}}{\rho_p c_g d_p}\left(1 + 0.23\sqrt{Re}\right)\ln\left[1 + \frac{c_g\left(T_g - T_p\right)}{h_{fg}}\right] \tag{6}$$

where, k_{ta} is the thermal conductivity of the gas and c_g is the specific heat capacity of the gas; the Reynolds number, *Re*, is given by eq.(2).

BOUNDARY CONDITIONS

Case A was used to validate the CFD simulation methodology with experimental results from Kieviet's[12] study and hence identical geometric and operating conditions were set. Kieviet employed a co-current, cylinder-on-cone short-form drying chamber; a pressure nozzle atomiser was located at the top of the chamber and the drying air entered through an annulus surrounding the spray. The outlet air line was a bent pipe mounted at the cone centre and was connected to the cyclone to separate the particles from the gas stream. Wall boundary conditions were set on all solid surfaces, along with inlet conditions for the gas feed and pressure outlet conditions for the main particle and gas exit streams. The pressure at the exit of the outlet pipe was set at a pressure 100 Pa lower than the inlet. The spray "injection" conditions are specified in Table 1. The particle size distribution was modelled using a Rosin-Rammler distribution with 30 particle classes chosen to represent the spray in the range 10 to 138 μm. The total number of particle tracks was selected as 1500. The feed liquid properties were based on an aqueous maltodextrin solution (42.5% solids). The remaining boundary conditions are given in Table 1.

In *Case B*, an air blast nozzle atomiser model was represented using the in-built model in the Fluent code; the initial particle size distribution was based on user provided inputs of nozzle diameter, feed liquid flow rate, air velocity and total number of particles. The atomising air has been included as a separate inlet stream, with a prescribed velocity, calculated from the measured air flow rate. The feed liquid was based on a 30% solids whey protein isolate solution. Wall

boundary conditions were set on all solid surfaces, along with inlet conditions for the gas feed and pressure outlet conditions for the exit stream. The outlet pressure was set 100 Pa lower than the inlet. The overall wall heat transfer coefficient for *Case B* was previously determined experimentally from an energy balance over the dryer. The full set of boundary conditions is given in Table 1.

The particle history data presented in the following sub-sections were extracted from the simulation results using an in-house post-processing computer program. A particle which hits the walls of drying chamber, was assumed to have "*escaped*", i.e. the particles are lost from the calculation at the point of impact with the wall.

RESULTS AND DISCUSSION

Experimental validation of simulated air velocity and temperature profiles for Case A: Short form spray dryer

Gas Velocity Profile without Spray Injection

The gas velocity magnitude profiles are plotted in Fig. 2 (a) and (b) at two different heights (z = 0.3 m and 2.0 m measured downwards from the ceiling) and compared with Kieviet's[12] experimental measurements and Huang *et al*.'s[8] simulation predictions. Data obtained in the X-Z planes are labelled as 'X' and Y-Z planes are labelled as 'Y' in Fig. 2 (a) and (b). The predictions from the current simulation agree well with Kieviet's[12] experimental results for the gas velocity magnitudes. The gas centreline velocity reduces as the gas travels axially down

the chamber: *e.g.* at z = 0.3 m the highest velocity magnitude is about 8 m/s, whereas, at z = 2.0 m it is only 6 m/s. The gas flow patterns are almost symmetric at z = 0.3 m (Fig. 2 a), but become more asymmetric at z = 2.0 m (Fig. 2 b) because of the bent outlet pipe (see Fig. 1) which reduces the area for gas flow on one side of the drying chamber, as commented on previously[8].

Comparison of the Gas Temperature Profile with Spray Injection

Fig. 3 (a) and (b) show predicted radial profiles for gas temperature at axial distances of z = 0.2 m and 1.4 m from the top of the chamber, in comparison with Kieviet's[12] experimental measurements. With the exception of the centreline data point at z = 1.4 m the predictions were in good agreement with the experimental results. In Kieviet's[12] experiments, the feed was atomised by using a pressure nozzle and this produced a hollow-cone spray. The temperature at the centreline axis was lower in comparison to the rest of the core region (Fig. 3 a), because this position was below the spray point. However, this did not occur at z = 1.4 m due to greater mixing of gas by this point (Fig. 3 b). The same result was shown by Huang *et al*.'s [8] model, which is also shown in Fig. 3.

Simulated particle histories for Case A

Radial Profiles of Particle Axial Velocity

The predicted radial profiles of particle axial velocity at z = 0.6 m and 2.0 m are shown in Fig. 4 (a) and (b) for four particle diameters of 17, 50, 75 and 100 μm which were selected to represent the behaviour of different particle size classes. The particle axial velocities are different from the gas velocities with the gas showing upward velocities outside of the central core region (also seen in simulations by Woo et al. [13]) in contrast to the particles which are predicted to travel downwards. In the core region of the chamber fewer data are shown for particle velocities because only a small number of particles entered this region due to the use of a hollow cone spray with a 76° spray angle. Where data exist for particles in the core region the particle velocities are higher than that of the gas. This can be attributed to the particles maintaining momentum from the spray jet [10]. The larger particles would be expected to maintain larger velocities [11], but this is not always observed in the simulation results and may be a result of the relatively small sample size giving sampling errors.

Radial Profiles of Particle Temperature

The predicted radial profiles of particle temperatures at z = 0.6 m and 2.0 m from the chamber top are shown in Fig. 5 (a) and (b). Significant wet-bulb depression is seen in the main spray region (r < 0.4 m) at z = 0.6 m except for the 17 μm diameter particles which have presumably already dried. Outside the core region (0.4 < r < 1.2 m) the particle temperatures are almost equal to the

gas temperatures, and relate to recirculating particles that have also dried. In the core region, particle temperatures at z = 0.6 m and z = 1 m (not shown in Fig. 5) were around 350 and 365 K respectively. Further down the chamber (z = 2 m), in the core, the particles dry out and approach the gas temperature (391 K). This result corroborates the widely held view that the outlet temperature has a greater effect on the temperature histories experienced by particles than the inlet air temperature.

Particle Residence Time Distributions

The particle trajectories were calculated in Fluent by integrating the equation of motion, eq.(1), over time, assuming gravity and drag to be the only significant terms. Particle residence time distributions (RTDs) were extracted from the simulation data by using an in-house post-processor, written in Excel VBA. The residence time (RT) can be divided into two parts namely, primary and secondary residence times. The primary RT is calculated from the time taken for particles leaving the nozzle to impact on the wall or leave at the outlet. For particles that hit the wall a secondary residence time can be defined as the time taken for a particle to slide along the wall from the impact position to the exit. This is based on an assumption that particles move with constant velocity along the wall from the impact position[12]. However, this assumption may not be accurate, as the sliding behaviour of powders differs at various wall positions. Furthermore, the layer of powder on the wall grows with time and is subject to intermittent detachment of pieces of the layer. Moreover, mechanical hammers are also often used to tumble the powders, so it is very difficult to calculate

representative constant sliding velocities of the particles. Hence, only primary RT results are given in this study.

Fig.6. shows trajectories of the particles and it can also be seen that dried particles tended to recirculate by the up flow of gas at the walls (the lighter colour of the trajectories indicates a longer particle primary residence time) Consequently, cold gas containing dried particles is mixed with down-flowing hot inlet gas and dried particles will be exposed to the high inlet gas temperatures. The overall primary RTD (for all particle diameters) is shown in Fig. 7. The observed minimum and maximum particle RTs are 0.4 s and 34.5 s respectively. The RTD curve shows a sharp peak at around 6 s (Fig. 7) and indicates that some particles have a long RT, due to recirculation. The average RT is 3.3 s, which is much lower than the gas residence time (22.4 s), because this RTD was calculated for the primary RT and the particles travel with a high velocity for a short period after leaving the atomiser. Zbicinski *et al*.[21] also concluded from their experimental results that there is no simple relation between gas and particle mean RTs. The RTDs of the different size classes of particles are shown in Fig. 8. Larger diameter particles have longer RTs than smaller particles. Smaller particles are more likely to follow the gas flow and thus exit the chamber in less time[14]. The same trend was observed by Kieviet[12] as well as Jin and Chen [14]. However, no direct measurements of primary RT are available to confirm the predictions of Fig. 8.

Particle Impact Positions

A knowledge of particle impact positions is important for the design and operation of spray-dryers as it influences the product quality. Particle impact positions were extracted from the CFD Lagrangian tracking data using the in-house post-processor, and are depicted in Fig. 9 (a) and (b), which show the top and front cross-sectional views of the simulated short-form dryer and Fig. 9c shows the percentage of particles impact positions. These figures indicate that a large fraction of the particles (50%) strike the conical part of the spray-dryer chamber and 23% of particles hit the cylindrical part of the wall, but only a small proportion (25%) of the particles come out of the outlet pipe line (the intended destination). A very small fraction (2 %) of particles hit the ceiling despite the large volume of re-circulated gas. Fig. 9c also shows some “incomplete” particles which refers to particles that are still in the chamber after 30 s, which is the timescale of the simulation for *Case A*. Here, an interesting point is that no particles are seen to come out of the main chamber outlet, but particles hitting the cone and/or cylindrical wall (73 %) should slide down to the main outlet aided by mechanical hammer operations.

Simulated gas and particle behaviour for Case B: Tall-form spray dryer

Case B is concerned with the CFD simulations relating to a tall-form spray-dryer used in experimental whey protein denaturation studies[15]. The simulation methodologies used were the same for *Cases A* and *B*. However, the tall-form spray dryer of *Case B* was constructed almost 25 years ago and there

were no options for measurements of velocity and gas/particle temperature inside the drying chamber. It was considered that the spray-dryer simulation methodology had been validated with the *Case A* study and hence may be applied with confidence to the *Case B* study. This simulation makes use of a wide range of particle diameters from 6 to 60 μm, but four particles sizes of 10, 20, 30 and 40 μm were selected as representative in Figs. 10 and 11.

Particle Axial Velocity at Various Radial Positions

The radial profiles of particle velocity at z = 0.4 m and 2.1 m are shown in Fig. 10 (a) and (b). In this simulation, the spray half angle is only 9° (solid cone) and hence there are many control volumes where no particles pass through. The particle axial velocities were almost equal to the gas velocity profiles. At z = 0.4 and 2.1 m the predictions show very similar axial velocities for all sizes of particles; the gas and particle velocities decrease with distance away from the nozzle, as the spray decelerates and the gas jet expands.

Radial Profiles of Particle Temperature

Fig. 11 (a) and (b) shows radial profiles of the particle temperature at z = 0.4 m and 2.1 m. Similar results are found to *Case A*. On the centreline at z = 0.4 m the 10 μm particles have a much higher temperature than the larger particles, because the latter are still drying. However, the fact that the 10 μm particle is hotter than the gas is curious, and may be the result of being transported out from an adjacent hot air region by eddy motions. At r = 0.1 m and z = 0.4 m the temperatures are relatively high for all particle sizes, due to the

high gas temperatures from the gas inlet (Fig. 11 a). This region may be responsible for high amounts of protein denaturation; here the particles are still wet, which is conducive to denaturation taking place. Outside the core ($r \geq 0.2$ m) all the particle temperature profiles closely follow the lower gas temperature of the recirculated gas. Fig. 11 (b) suggests that particles are totally dried as they are very close to the gas temperature. In the simulation a constant drying rate regime is used, which will tend to over-predict drying rates (compared to real particles which will experience a falling rate period). This assumption will result in the complete drying of particles at shorter residence times than would be the case for real particles undergoing a falling rate drying process. Thus in practice particle temperatures may still be a few degrees (0-3 K) cooler than in the simulation.

Particle Residence Time Distributions

Fig. 12 shows particle trajectories for *Case B* in which some dried particles can be seen to recirculate with the gas phase. These particles rise up the walls and are entrained back into the jet leaving the nozzle. This may cause protein denaturation as recirculated particles are exposed to higher inlet gas temperatures without wet bulb protection. The overall primary residence time distribution of all particles is shown in Fig. 13 which indicates that a wide range of RT is predicted. The minimum and maximum RT were 0.43 s and 27 s respectively. The average RT is 4.2 s, which is much lower than the gas mean residence time (22 s).

Particle Impact Positions

The particle impact positions for *Case B* are depicted in Fig. 14. These indicate that 65 % of the particles strike the cylindrical part of the wall and 9.6 % of particles hit the conical part of the wall, but only a small proportion (8%) of the particles come out of the outlet pipe line. Less than 1% of particles impact on the ceiling, as recirculation of gas only took place on a large scale at the bottom of the chamber. The reduced proportion of particles reaching the exit pipe compared to *Case A* contributes to an increase in the particle RT inside the chamber. In turn this affects the product quality, especially for proteins, where dried particles may be exposed to the highest temperature for a long time; the degree of whey protein denaturation increases with the temperature and holding time. This findings supports the experimental results[15], where some denaturation of whey proteins has been found even at low outlet temperatures.

CONCLUSIONS

A three-dimensional CFD model for a short-form spray dryer was developed and compared with published experimental results and predictions. The comparison study shows good agreement between the model and published experimental and prediction results for gas velocity and temperature profiles. The study predicts that the particle residence time is not simply related to the gas residence time, and also confirms that particle size distribution is important for achieving higher evaporation rates because, smaller mean diameter particles dry faster. As a result, small particles lose their wet-bulb protection sooner and experience the high temperatures of the surrounding gas. In *Case A*, the wider

spray angle provided a broader distribution of particle trajectories inside the chamber and that led to higher rates of heat and mass transfer.

The successful validation of the short-form spray dryer (*Case A*) study results gives confidence in the predictions for modelling the tall-form dryer (*Case B*). The *Case B* model predicts fewer particles travelling to the dryer exit tube which may adversely affect product quality (such as increased denaturation of proteins). The tall-form dryer is predicted to have longer particle primary residence time and this may also lead to more denaturation and insolubility of proteins. These results confirm that the outlet dryer temperature has more influence on the particle thermal history than the inlet temperature. However a zone where the spray meets the hot air inlet may be responsible for much of the denaturation that occurs in a spray dryer.

These short-form and tall-form spray dryer studies suggest that an increase in the chamber diameter: (1) may reduce the particle deposition rates on the cylindrical wall (e.g. in *Case A*), and (2) can accommodate a wider atomiser spray angle, which improves heat and mass transfer rates. Hence, this study concludes that a short-form dryer with a simple bottom outlet is most likely to be suitable for the drying of heat sensitive products such as proteins.

ACKNOWLEDGEMENTS

We gratefully acknowledge the Commonwealth Scholarship Commission, UK for the award of a Commonwealth Scholarship to CA, which enabled this work to be carried out.

REFERENCES

1. Masters, K. *Spray Drying Handbook;* Longman Scientific and Technical; Harlow, 1991.

2. Mujumdar, A. S. *Handbook of Industrial Drying*; Marcel Dekker; New York, 1987.

3. Anandharamakrishnan, C. Computational fluid dynamics (CFD) – applications for the food industry. Indian Food Industry **2003,** *22* (6), 62-68.

4. Norton, T.; Sun D.W. Computational fluid dynamics (CFD) - an effective and efficient design and analysis tool for the food industry: A review. Trends in Food Science and Technology **2006**, *7*, 600-620.

5. Langrish, T.A.G.; Oakley, D.E.; Keey, R.B.; Bahu, R.E.; Hutchinson, C.A. Time-dependent flow patterns in spray dryers. Trans I Chem E, Part A **1993**, *71*, 355-360.

6. Zbicinski, I. Development and experimental verification of momentum, heat and mass transfer model in spray drying. The Chemical Engineering Journal **1995**, *58*, 123-133.

7. Huang, L.X.; Kumar, K.; Mujumdar, A.S. A parametric study of the gas flow patterns and drying performance of co-current spray dryer: Results of a computational fluid dynamics study. Drying Technology **2003**, *21*(6), 957-978.

8. Huang, L.X.; Kumar, K.; Mujumdar, A.S. A comparative study of a spray dryer with rotary disc atomizer and pressure nozzle using computational fluid dynamic simulations. Chemical Engineering and Processing **2006**, 45, 461-470.

9. Langrish, T.A.G.; Fletcher, D.F. Spray drying of food ingredients and applications of CFD in spray drying. Chemical Engineering and Processing 2001, *40*, 345-354.

10. Crowe, C.T.; Sharam, M.P.; Stock, D.E. The particle source in cell (PSI-Cell) model for gas-droplet flows, Journal of Fluid Engineering **1977**, *9*, 325-332.

11. Papadakis, S.E.; King, C.J. Air temperature and humidity profiles in spray drying. 1. Features predicted by the particle source in cell model. Industrial Engineering Chemistry Research **1988**, *27*, 2111-2116.

12. Kieviet, F.G. *Modeling Quality In Spray Drying,* Ph.D. thesis; Eindhoven University of Technology; Netherlands, 1997.

13. Woo. M.W.; Daud, W.R.W.; Majumdar, A.S.; Wu, Z.H.; Talib, M.Z.M.; Tasirin, S.M. CFD evaluation of droplet drying models in a spray dryer fitted with rotary atomizer. Drying Technology **2008**, *26*(10), 1180-1198.

14. Jin, Y.; Chen, X.D. Numerical study of the drying process of different sized particles in an industrial scale spray dryer. Drying Technology **2009**, *27*(3), 371-381.

15. Anandharamakrishnan, C.; Rielly, C.D.; Stapley, A.G.F. Effects of process variables on the denaturation of whey proteins during spray-drying. Drying Technology **2007**, *25*, 799-807.

16. *Fluent User Guide*; Fluent Inc.: Lebanon, NH, **2005**.

17. Langrish, T.A.G.; Zbicinski, I. The effects of air inlet geometry and spray cone angle on the wall deposition rates in spray dryer. Trans I ChemE, Part A **1994**, *72*, 420-430.

18. Morsi, S.A. ; Alexander, A.J. An investigation of particle trajectories in two-phase flow systems. Journal of Fluid Mechanics **1972**, *55* (2), 193-208.

19. Perry, R.H.; Chilton, C.H. *Chemical Engineers Handbook*; McGraw-Hill; London, 1984.

20. Incropera, F.P.; Dewitt, D.P.; Bergman, T.L.; Lavine, A,S. *Fundamentals of Heat and Mass Transfer*; John Wiley & Sons; New York, 2007.

21. Zbicinski, I.; Strumillo, C.; Delag, A. Drying kinetics and particle residence time in spray drying. Drying Technology **2002**, *20* (9), 1751-1768.

Table 1 Boundary conditions

	Case A	*Case B*	
Inlet Air			
Air inlet temperature	468	444	K
Air mass flow rate	0.336	0.063	kg/s
Air axial velocity	7.5	8.87	m/s
Air radial velocity	-5.25	–	m/s
Air total velocity	9.15	–	m/s
Outlet Condition			
Outflow & reference pressure	–100	–100	Pa
Turbulence inlet conditions			
Turbulence k-value	0.027	0.29	m^2/s^2
Turbulence ε-value	0.37	0.51	m^2/s^3
Liquid spray from nozzle			
Liquid feed rate (spray rate)	0.0139	0.00203	kg/s
Feed Temperature	300	293	K
Spray angle	76°	18°	
Minimum droplet diameter	10	–	μm
Maximum particle diameter	138	–	μm
Average particle diameter	70.5	–	μm
Particle velocity at nozzle	59	–	m/s
Rosin-Rammler parameter	2.05	–	
Chamber wall conditions			
Chamber wall thickness	0.002	0.002	m
Wall material	Steel	Steel	
Overall wall heat transfer coefficient	3.5	3.5	W/m^2K
Air temperature outside wall	300	293	K
Interaction between wall and particle	escape	escape	

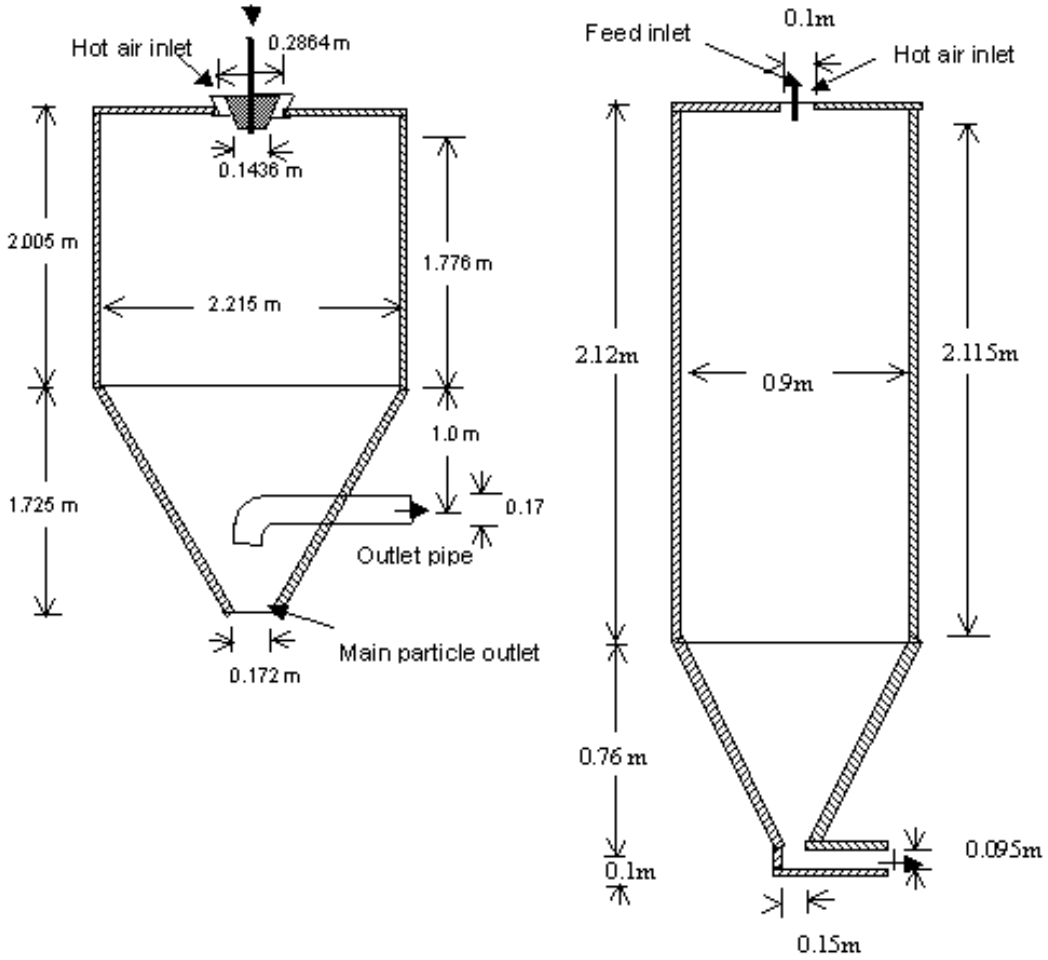

Fig. 1. Spray-dryer geometries: short form (left, *Case A*) and tall form dryer (right, *Case B)*.

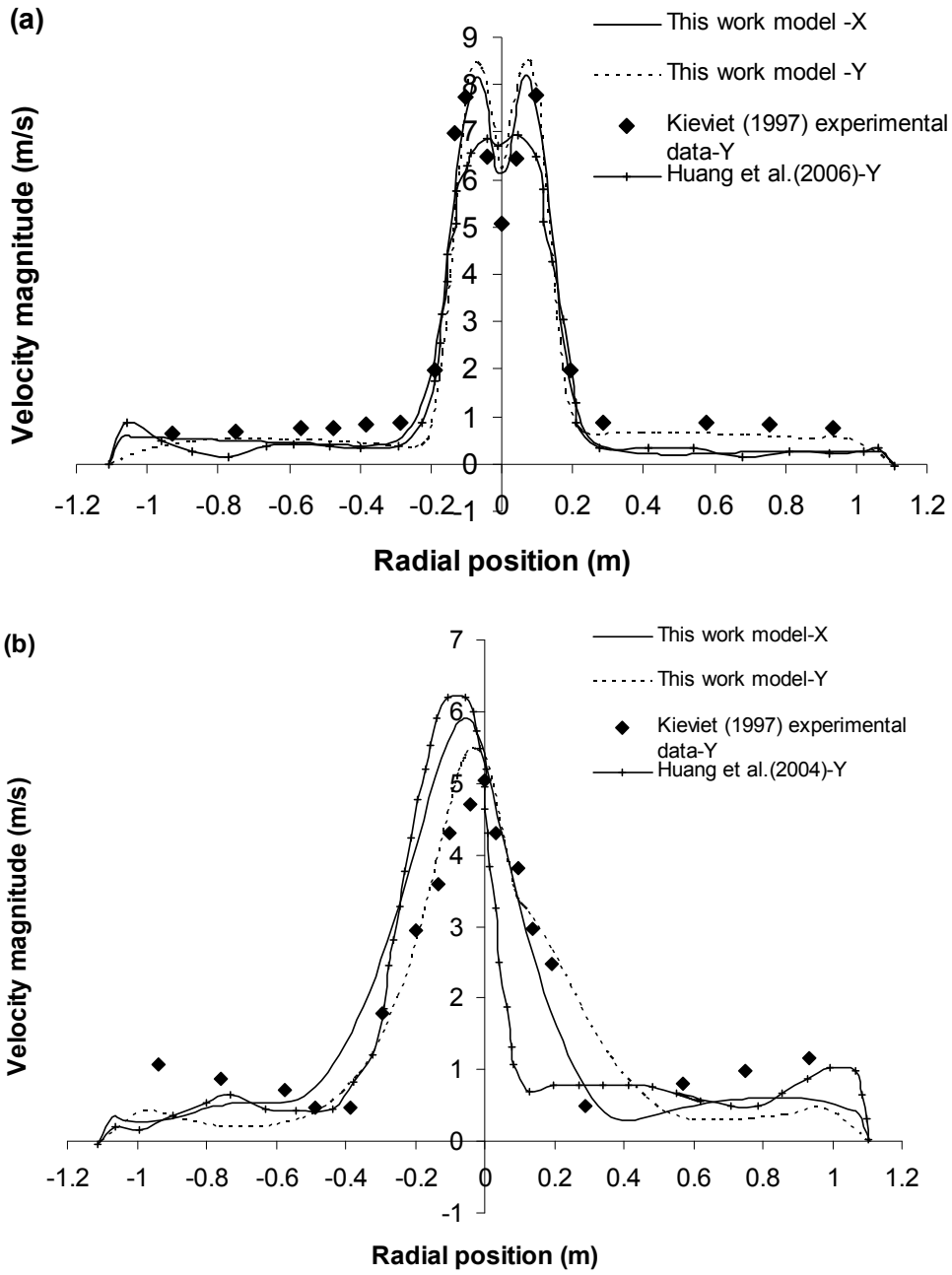

Fig. 2. Comparison of the gas velocity magnitude between this work's CFD model, Kieviet's (1997) measurements and Huang *et al*.'s (2006) predictions for *Case A* at (a) z = 0.3 m and (b) z = 2.0 m.

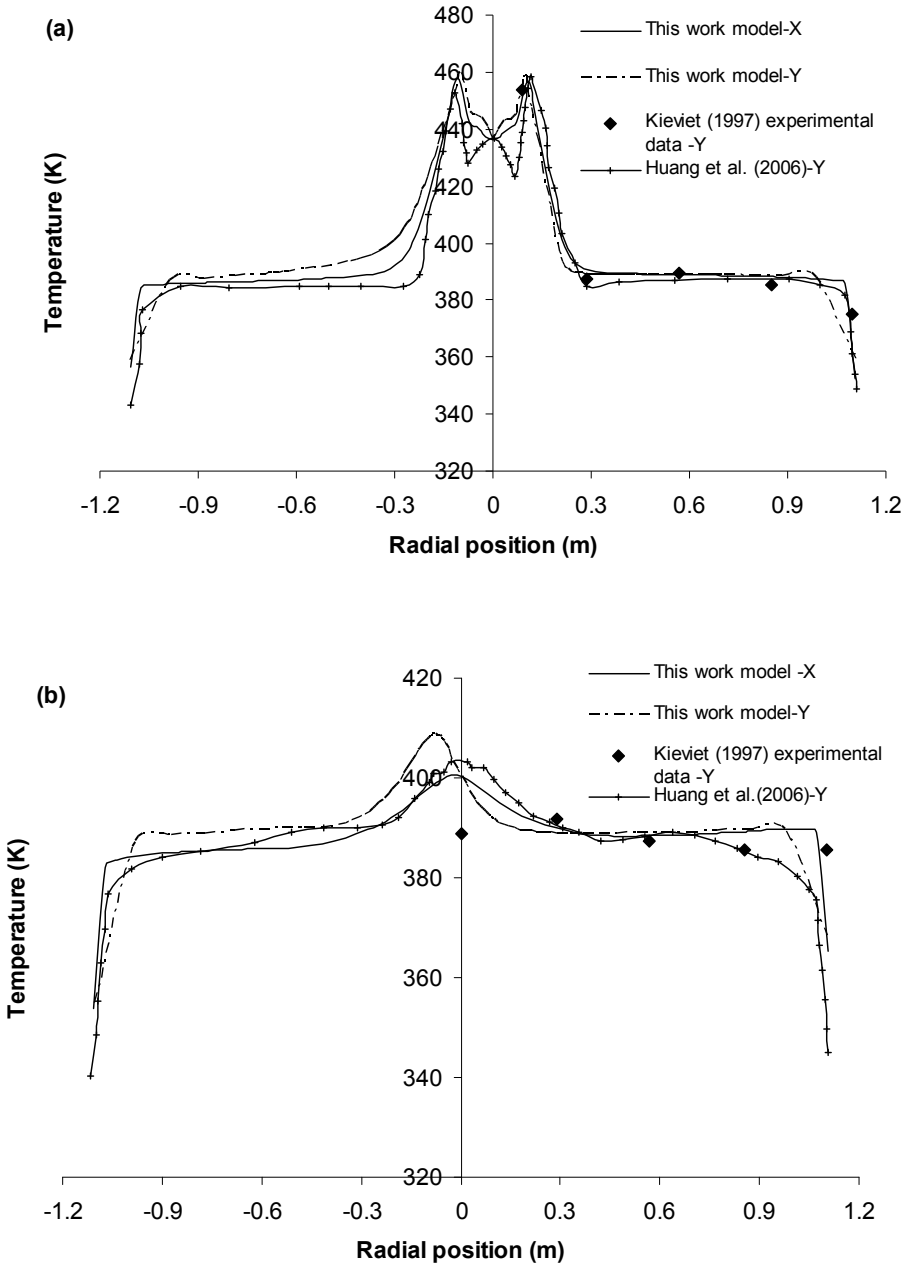

Fig. 3. Comparison of gas temperature profiles between this work's CFD model, Kieviet's (1997) measurements and Huang *et al*.'s (2006) predictions for *Case A* at (a) z = 0.2 m and (b) z = 1.4 m.

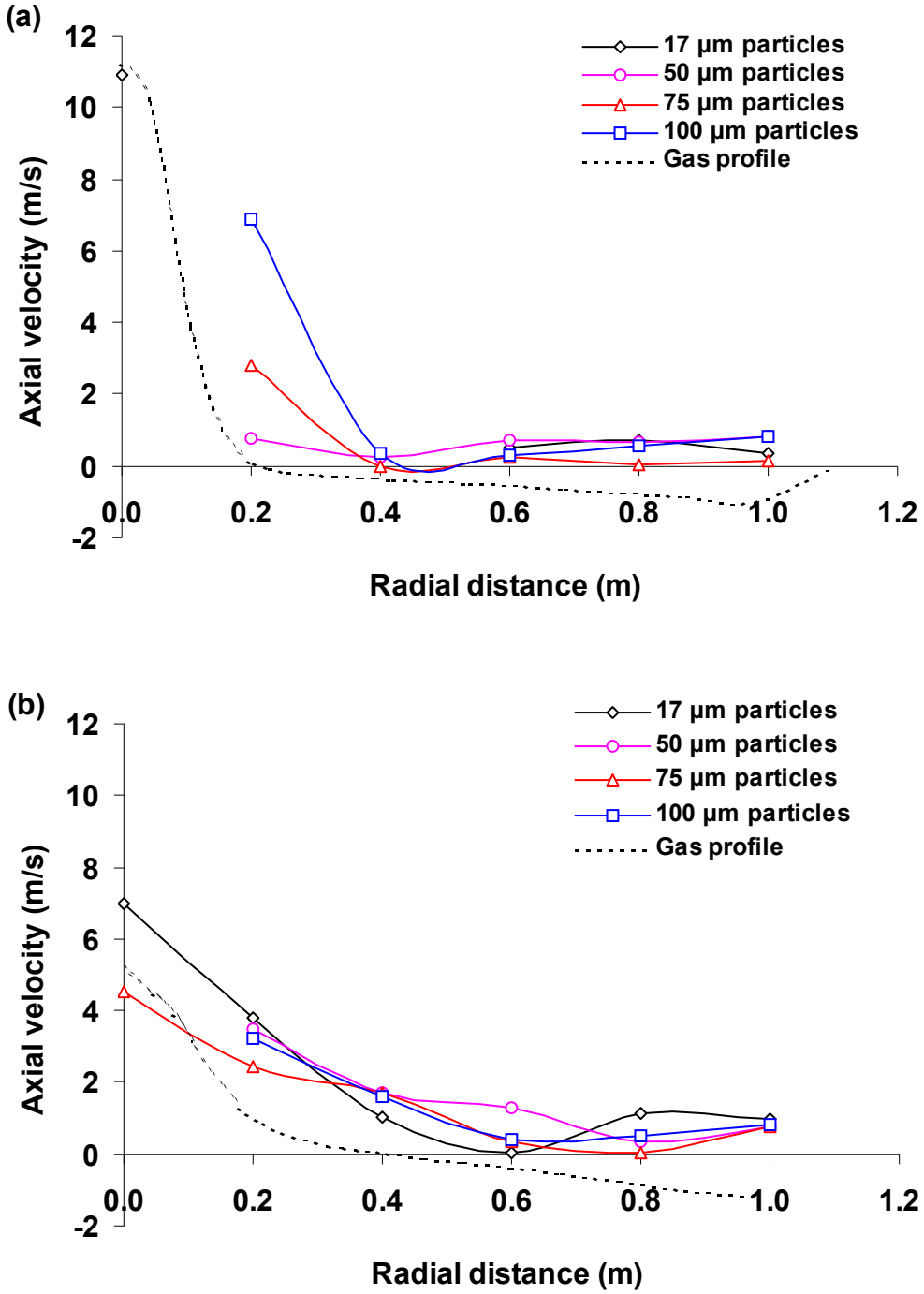

Fig. 4. Radial profiles of the particle axial velocities for *Case A* at (a) *z* = 0.6 m and (b) z = 2.0 m.

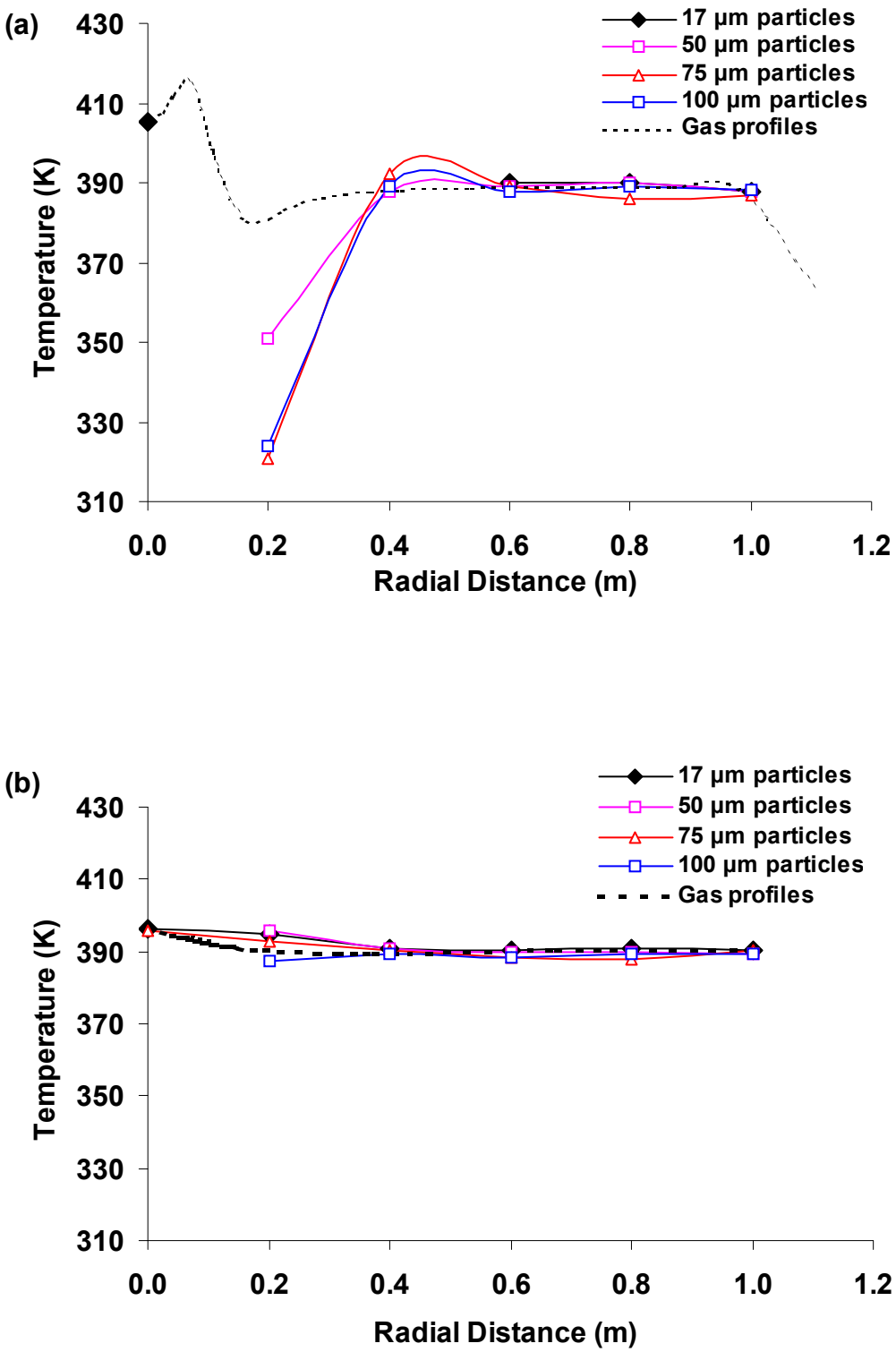

Fig. 5. Simulated radial temperature profiles for *Case A* at (a) z = 0.6 m and (b) z = 2.0 m.

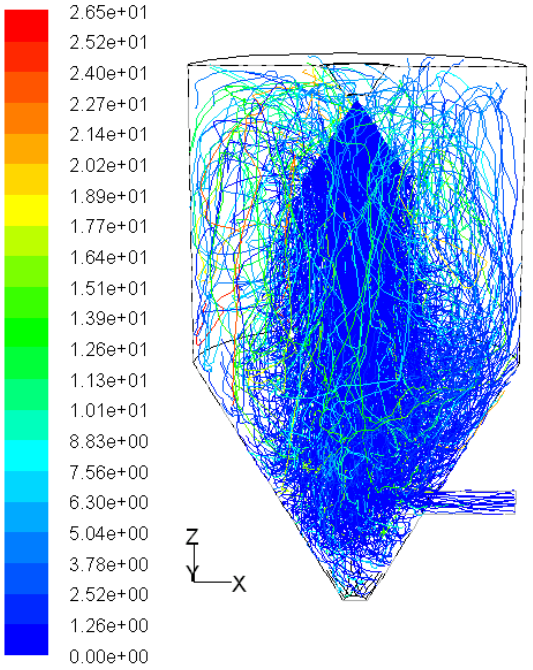

Fig. 6. Particle trajectories coloured by residence time (s) (Case A)

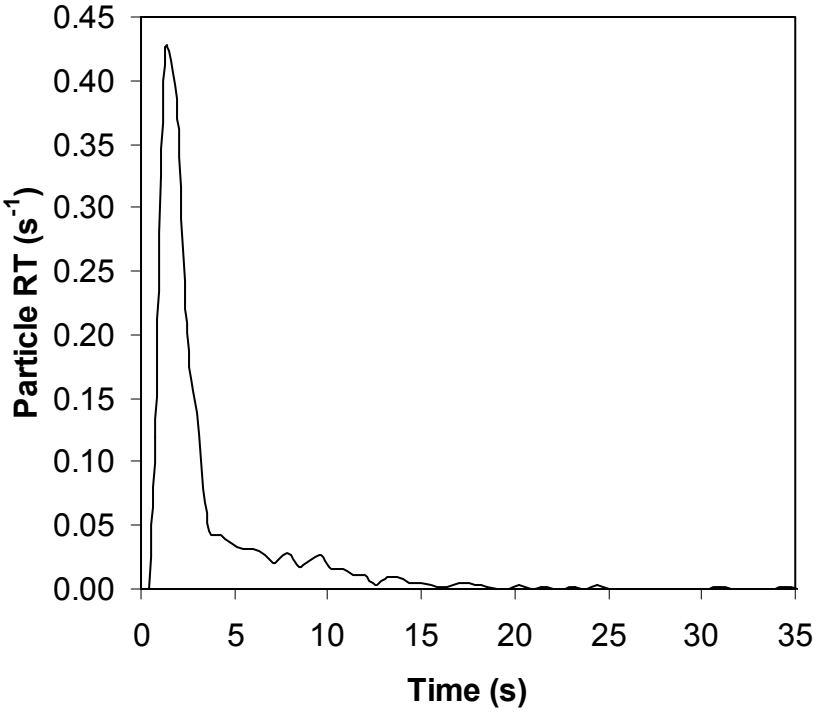

Fig. 7. Particle overall primary RTD (*Case A*) for the whole size distribution.

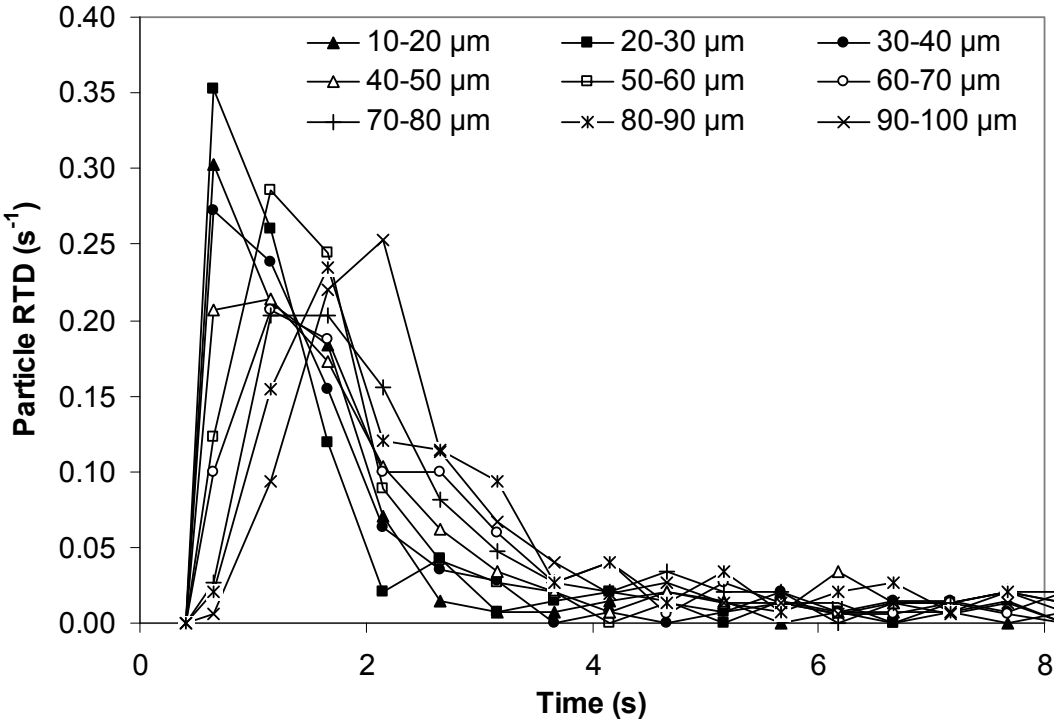

Fig. 8. Simulated residence time distributions for different particle diameters (Case A).

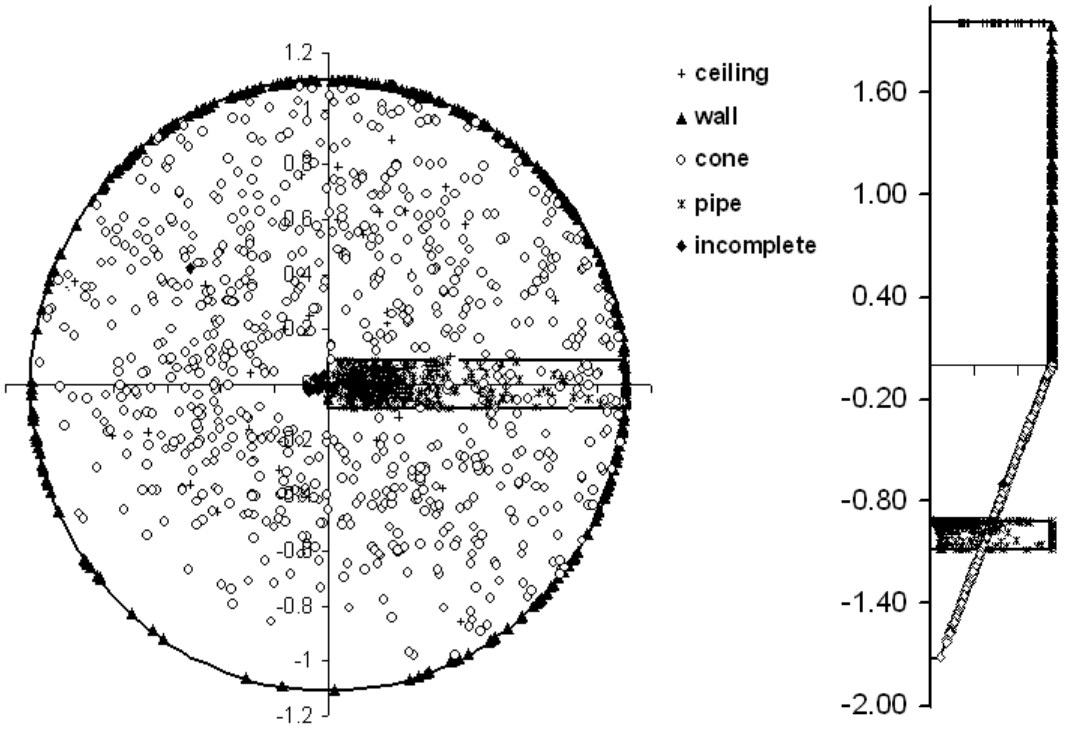

(a) (b)

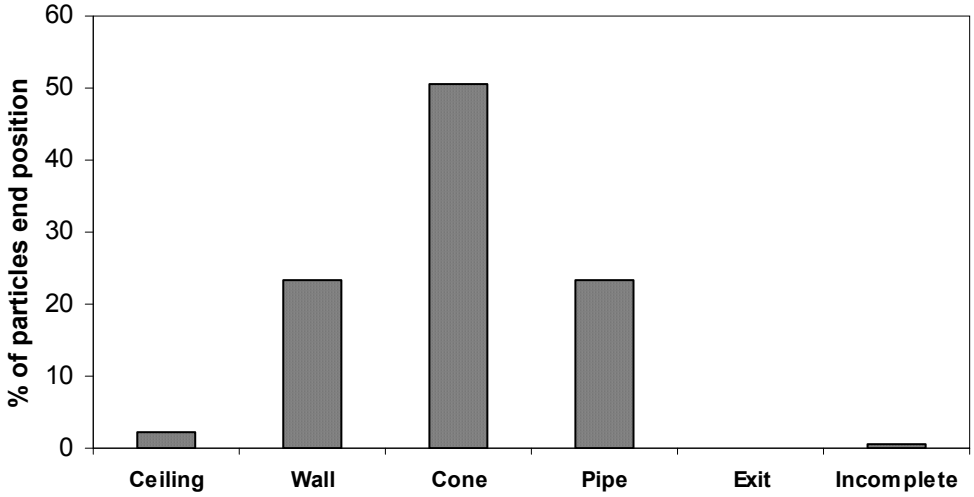

(c)

Fig. 9. Particle impact positions (*Case A*): (a) top view (b) front view (c) % of particles end position (Incomplete" refers to particles still in the chamber after 30 s - the timescale of the simulation).

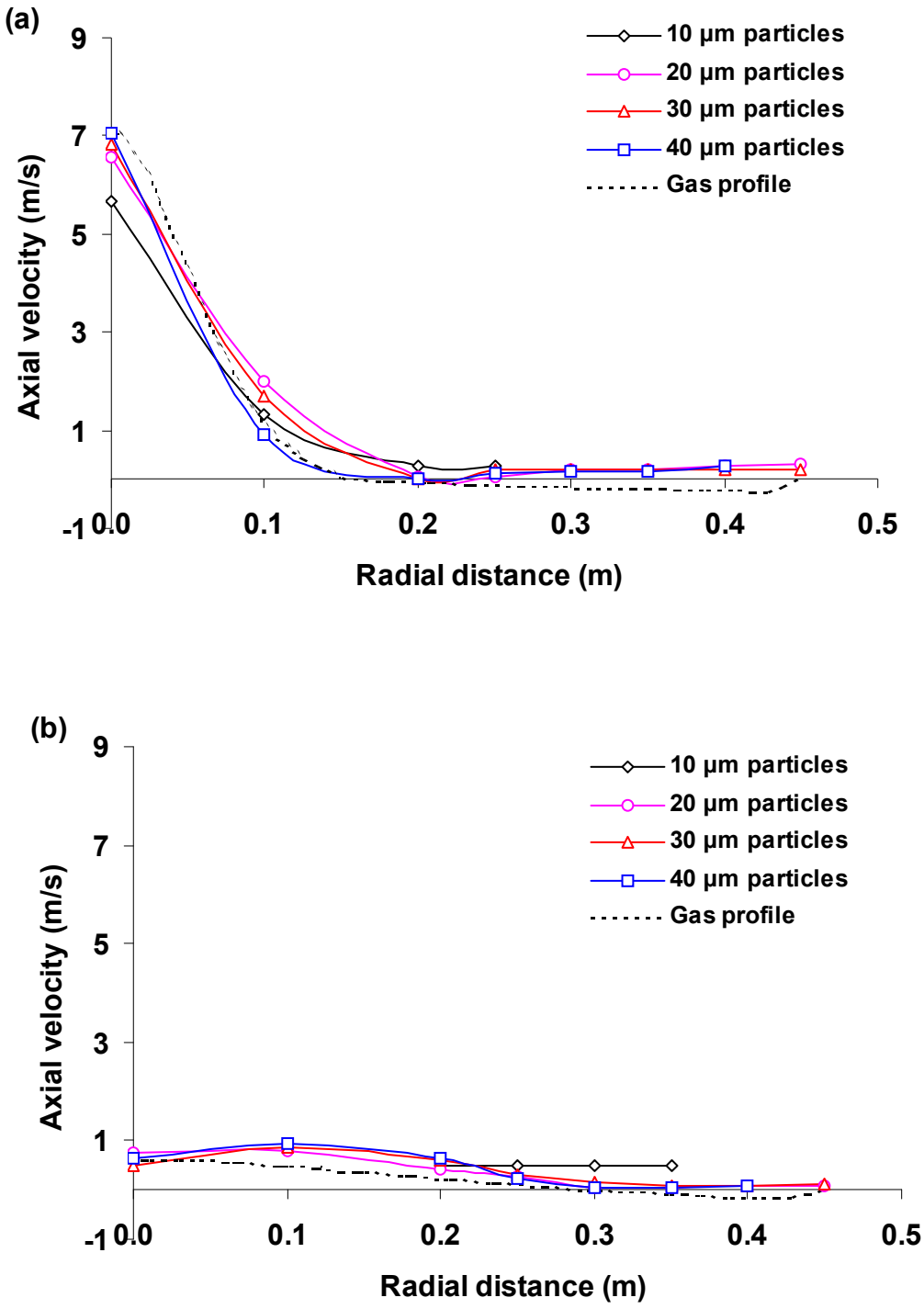

Fig. 10. Simulated gas and particle axial velocity profiles for *Case B* at (a) z = 0.4 m and (b) z = 2.1 m.

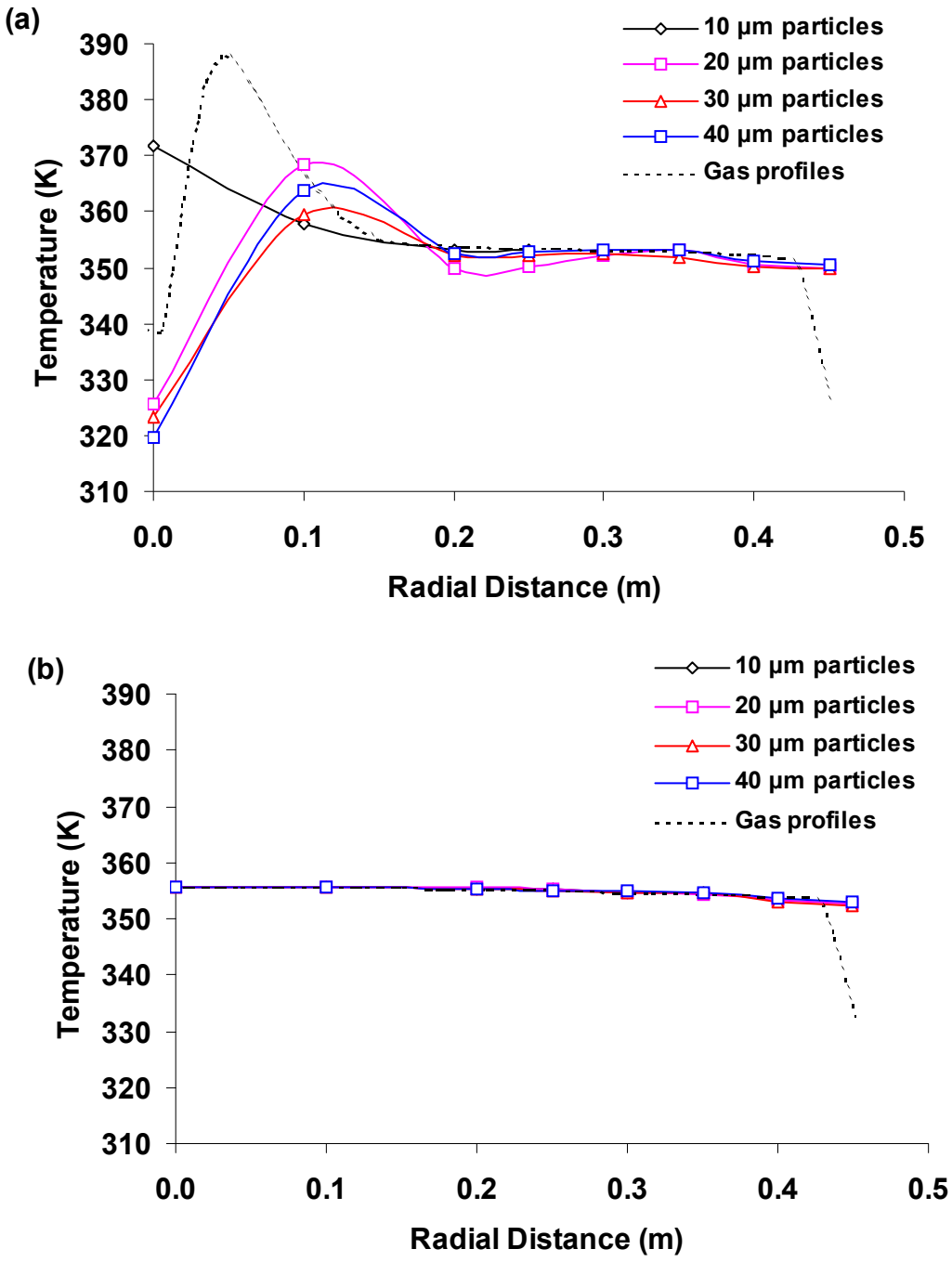

Fig. 11. Simulated gas and particle temperatures vs radial distance for *Case B* at (a) z = 0.4 m and (b) z = 2.1 m.

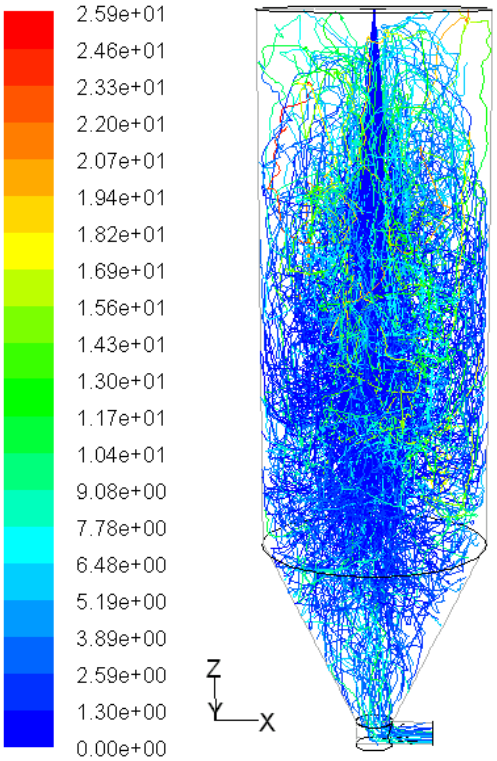

Fig. 12. Particle trajectories coloured by residence time (s) (*Case B*).

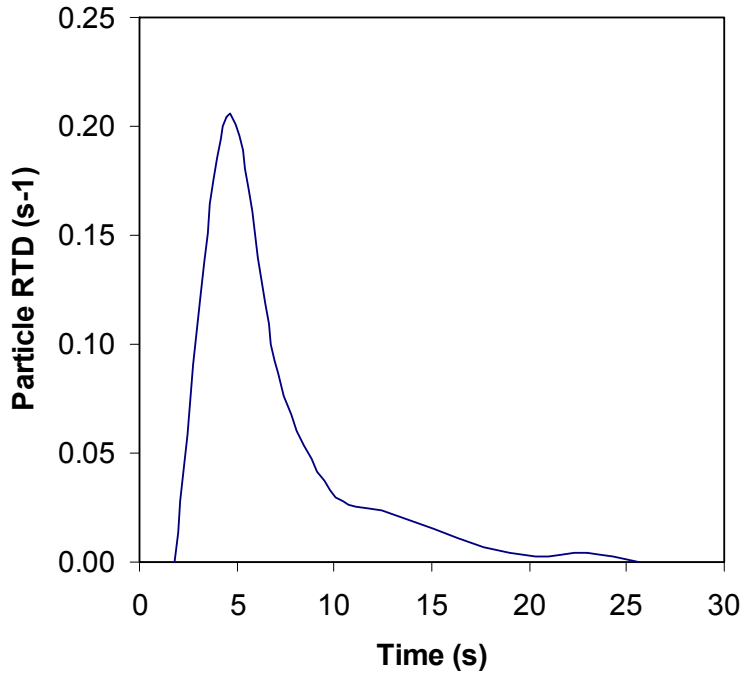

Fig. 13. Overall particle primary RTD (*Case B*) for the whole size distribution.

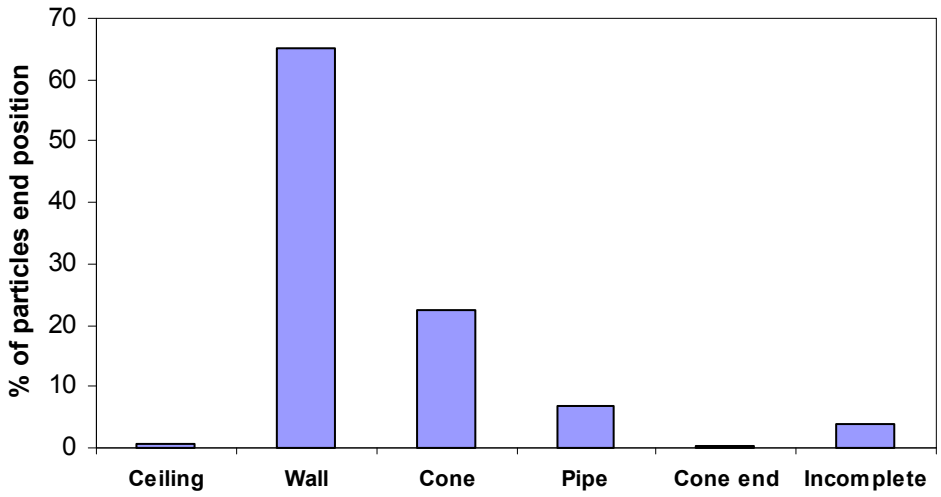

Fig. 14. Particle impact positions on wall. “Incomplete” means that particles are still in the chamber after 30 s (the timescale of the simulation for *Case B*).